

# Roles of orbital as a nexus between optical and magnetic properties in cubic $RMnO_3$ ( $R = \text{La, Pr, Nd, Gd, Tb}$ )

M. W. Kim<sup>1</sup>, S. J. Moon<sup>1</sup>, J. H. Jung<sup>2</sup>, Jaejun Yu<sup>3</sup>, Sachin Parashar<sup>1</sup>, P. Murugavel<sup>1</sup>, and T. W. Noh<sup>1\*</sup>

<sup>1</sup>*ReCOE & School of Physics, Seoul National University, Seoul 151-747, Korea*

<sup>2</sup>*Department of Physics, Inha University, Incheon 402-751, Korea*

<sup>3</sup>*CSCMR & School of Physics, Seoul National University, Seoul 151-747, Korea*

We investigated the *ab*-plane absorption spectra of  $RMnO_3$  ( $R = \text{La, Pr, Nd, Gd, and Tb}$ ) thin films. As the  $R$ -ion size decreases, we observed a drastic suppression of the 2 eV peak, *i.e.* the inter-site optical transition between spin- and orbital-aligned states across the Mott gap. We found that both lattice distortion and the corresponding orbital mixing of the ordered orbital state should play an important role in the 2 eV peak suppression. We also found that the 2 eV spectral weight is proportional to the  $A$ -type antiferromagnetic ordering temperature, which suggests that the magnetic interaction might be sensitively coupled to the orbital mixing.

PACS numbers: 75.70.-i, 77.90.+k, 78.20.-e

$LaMnO_3$  has been known as a mother compound of the colossal magnetoresistance (CMR) manganites, where charge, spin, lattice, and orbital degrees of freedom interplay with each other to determine their intriguing physical properties [1, 2].  $LaMnO_3$  has an orthorhombic structure with four  $3d$ -electrons: three  $t_{2g}$  and one  $e_g$  electrons. Since three  $t_{2g}$  electrons form an orbitally closed shell, many physical properties are believed to be determined by its  $e_g$  electron. In its ground state,  $LaMnO_3$  is a Mott-insulator [3, 4, 5] with the  $A$ -type spin and the  $C$ -type orbital orderings, which are schematically drawn in Figs. 1(a) and 1(b), respectively. The antiferromagnetic (AFM) ordering temperature  $T_N$  is about 140 K, and the orbital ordering temperature is around 800 K. The occurrence of the spin- and orbital-ordered state has been understood in terms of the cooperative Jahn-Teller (JT) transition [6].

Rare-earth substitutions of the La ion provide an intriguing phase diagram for  $RMnO_3$  ( $R = \text{rare-earth ion}$ ) [7], as illustrated in Fig. 1(c). As the  $R$ -ion size  $r_R$  decreases, the crystal structure of  $RMnO_3$  changes from orthorhombic ( $R = \text{La-Dy}$ ) to hexagonal ( $R = \text{Ho-Lu}$ ).  $TbMnO_3$  and  $DyMnO_3$  are located near the structural phase boundary, and they have attracted lots of attention recently due to their complicated low temperature magnetic states and multiferroic properties [8]. On the other hand, the magnetic properties of the orthorhombic perovskite  $RMnO_3$  ( $R = \text{La-Tb}$ ) has a rather simple  $R$ -dependence:  $T_N$  decreases with decreasing  $r_R$ . Structural deformations, such as buckling and distortion of the  $MnO_6$  octahedra, also increase. According to the Goodenough-Kanamori rule [6, 9], the orbital overlap of electrons should be crucial in determining the magnetic interaction. The rule takes into account the overlap in terms of the Mn-O-Mn bond angle  $\phi$ . However, the rapid decrease of  $T_N$  with the  $R$ -ion substitution is rather unexpected, since the change of  $\phi$  is less than  $10^\circ$ . In addition to the lattice distortion due to the  $\phi$  variation, a neutron scattering measurement showed that the  $e_g$  electron state

should have a mixed character of  $|3z^2 - r^2\rangle$  and  $|x^2 - y^2\rangle$  orbitals and that the degree of orbital mixing varies systematically with  $r_R$  [10]. This orbital mixing could also affect the orbital overlap of electrons. Therefore,  $RMnO_3$  ( $R = \text{La-Tb}$ ) is an ideal system to investigate roles of the lattice distortion and the orbital mixing in numerous physical properties.

Optical spectroscopy has been known to be a powerful tool to investigate the orbital degrees of freedom [3, 4, 11, 12]. In this Letter, we report the *ab*-plane optical responses of epitaxial  $RMnO_3$  ( $R = \text{La, Pr, Nd, Gd, and Tb}$ ) films. We find that the spectral weight of the optical transition across the Mott gap, located around 2 eV, decreases rapidly as  $r_R$  decreases. This dramatic reduction of the spectral weight cannot be explained in terms of the conventional model based on the structural variations. We demonstrate that the spectral weight change could be explained by taking account of the structural distortion, *i.e.*, the change of  $\phi$ , and the orbital mixing. We also find that the measured spectral weight change is proportional to the variation of  $T_N$ .

High quality  $RMnO_3$  ( $R = \text{La, Pr, Nd, Gd, and Tb}$ ) thin films were grown on double-side-polished  $(LaAlO_3)_{0.3}(SrAl_{0.5}Ta_{0.5}O_3)_{0.7}$  substrates by using the pulsed laser deposition. From x-ray diffraction measurements, it was found that all the films grew epitaxially with their  $c$ -axis perpendicular to the film surfaces. Details of the film growth and their characterization were reported elsewhere [13]. Transmission spectra of the films were measured from 0.4 to 4.0 eV by using a grating spectrophotometer. The absorption coefficients were determined by taking the logarithm of the transmittance, subtracting that of the substrate, and dividing by the film thickness. Since the normal-incident optical geometry was used, the absorption spectra should come from the *ab*-plane responses of the films. Figure 2(a) shows the absorption spectra  $\alpha(\omega)$  of  $RMnO_3$  at room temperature, where all the samples should be in the  $C$ -type orbital ordered state [14]. The spectra of  $LaMnO_3$  are

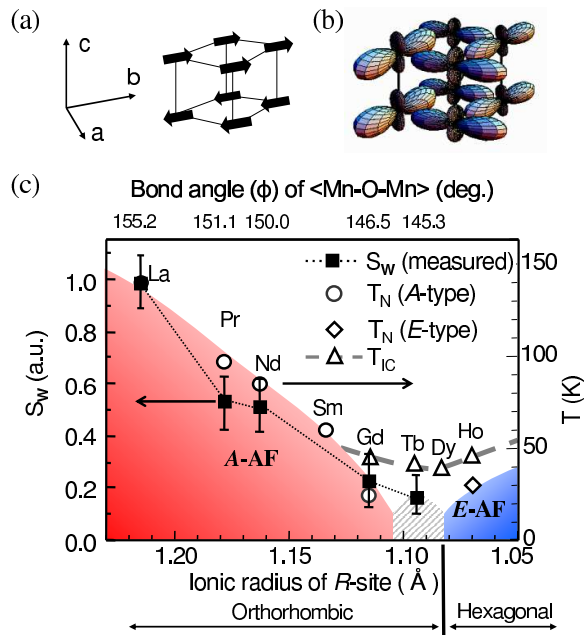


FIG. 1: (color online). (a) The A-type spin and (b) the C-type orbital ordering pattern of electrons at the Mn-sites in  $\text{LaMnO}_3$ . (c) A schematic magnetic phase diagram of  $\text{RMnO}_3$ , redrawn from Ref. [7]. The spectral weight of 2 eV peak,  $S_W$  (the solid square), shows similar R-ion size dependence with the A-type AFM ordering temperature ( $T$ ) (the open circles). The E-type AFM ordering  $T$  (the open diamonds) and the incommensurate spin ordering  $T$  (the open triangles) are also shown. The hatched area represents the region where the commensurate spin order and ferroelectric property emerges.

composed of a peak near 2 eV and much stronger absorption peaks above 3 eV. The higher energy absorption features come from the charge transfer transition from O  $2p$  to Mn  $3d$  [3, 15]. After long debates, numerous recent experiments clearly demonstrated that the 2 eV peak should be interpreted as an inter-site transition across the Mott gap in the orbitally degenerate Hubbard model (ODHM) [3, 4, 5]. As shown in Figs. 1(a) and 1(b), the correlation-induced transition within the  $ab$ -plane should occur between the  $e_g$  electron states at the neighboring sites in the ferromagnetic-spin (FM) and antiferro-orbital (AFO) configuration [3, 4, 16]. The absorption spectra of other  $\text{RMnO}_3$  have very similar spectral features. As  $r_R$  decreases,  $\alpha(\omega)$  for the charge transfer transition above 3 eV is nearly independent of the R-ion, however,  $\alpha(\omega)$  for the correlation-induced 2 eV peak

becomes strongly suppressed. To obtain more quantitative information, we estimated the spectral weight  $S_W$  by subtracting the charge transfer transition background and integrating  $\alpha(\omega)$  from 0.2 to 2.7 eV. The experimentally determined  $S_W$ , marked as the solid squares in Fig. 2(b), becomes drastically suppressed with decreasing  $r_R$ .

Such a dramatic decrease of  $S_W$  is rather unexpected. All the  $\text{RMnO}_3$  compounds, studied in this work, have the same orthorhombic crystal structure and the same spin/orbital ordering pattern, but only with a relatively small variation of  $\phi$ . Let us look into the possible role of the structural variations of  $\text{RMnO}_3$  in the large  $S_W$  change. According to the chemical grip estimate [17], the inter-site transition between the  $d$  states can vary approximately as  $\cos^4\phi$ . As shown in Fig. 2(b), the contribution of the structural variations to the  $S_W$  change could be as large as 30%, but is still much smaller than the experimentally observed  $S_W$  changes. Therefore, the electronic structure change due to the structural variation alone cannot explain the large suppression of  $S_W$ . To elucidate the origin of the 2 eV peak spectral change, we applied the Fermi-Golden rule and evaluate the corresponding matrix element. Within the electric dipole approximation[18],  $S_W$  becomes proportional to  $|\langle\psi_f| -i\hbar\nabla|\psi_i\rangle|^2$ . This matrix element can be approximated by the second order perturbation, similarly to the superexchange process, through the oxygen  $p$  orbitals:

$$S_W \propto |\langle\psi_f|\nabla|\psi_i\rangle|^2 \sim \left| \sum_{\alpha} \langle\psi_f|p_{\alpha}\rangle \langle p_{\alpha}|\psi_i\rangle \right|^2 / \Delta, \quad (1)$$

by assuming that the energy gap  $\Delta$  remains almost unchanged[19]. Here  $|\psi_i\rangle$  and  $|\psi_f\rangle$  represent the wavefunctions of the initial occupied and the final unoccupied Mn  $e_g$  orbitals, respectively, of the transition considered.  $|p_{\alpha}\rangle$  ( $\alpha = x, y, z$ ) represents the oxygen  $p$  orbitals which bridge the Mn  $e_g$  orbitals. For the 2 eV peak, the matrix element can be estimated by the inter-site transition from the occupied  $e_g$  state at one site to the unoccupied  $e_g$  state at the neighboring site with the FM/AFO configuration, as shown in the inset of Fig. 2(a).

First, let us consider the contribution of the Mn-O-Mn bond angle change in the matrix element. As shown in Fig. 3(a), the buckling of the  $\text{MnO}_6$  octahedra in the  $\text{GdFeO}_3$  type lattice will cause a decrease in  $\phi$ . Without the buckling (*i.e.*  $\phi \simeq 180^\circ$ ), the larger lobe of the  $|3x_1^2 - r_1^2\rangle$ -type orbital of a  $\text{Mn}^{3+}$  site is aligned to face the smaller lobe of the neighboring orbital orthogonally, as shown in Fig. 1(b). As the buckling is turned on, the orbital lobe of an electron at one site will rotate with respect to that at the neighboring site, which will result in a reduction in the inter-site hopping amplitude and thereby a decrease in  $S_W$ . To evaluate the changes in  $|\psi_i\rangle$  and  $|\psi_f\rangle$  quantitatively, the rotation of the orbitals in the  $ab$ -plane was formulated in terms of the rotational transformation of the local  $(x_2, y_2)$  coordinates by  $\phi$  with respect to the local  $(x_1, y_1)$  coordinates, as shown in Fig.

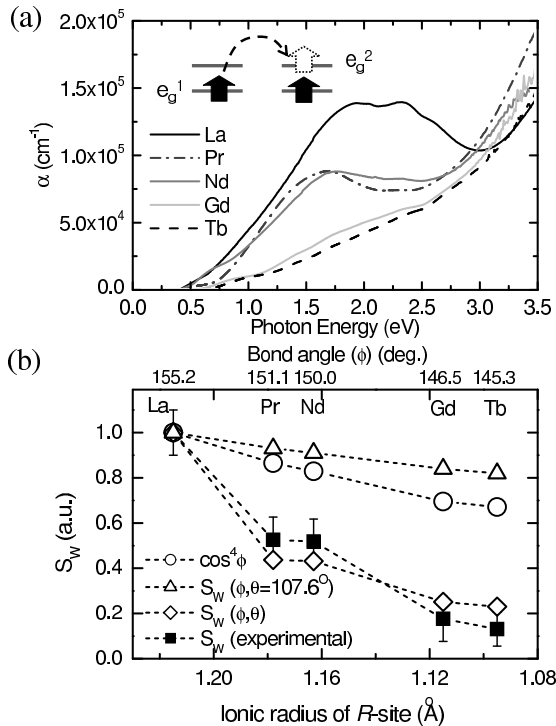


FIG. 2: (a) Absorption spectra of  $RMnO_3$  ( $R = \text{La, Pr, Nd, Gd, and Tb}$ ) thin films at room  $T$ . The inset schematically represents the inter-site transition corresponding to the 2 eV peak. (b) The experimental  $S_W$  (the solid squares) is compared with the calculation results: the simple estimation of bandwidth change ( $\sim \cos^4 \phi$ ) (the open circles), our model calculation for various  $\phi$  by using the orbitals of  $\text{LaMnO}_3$ , *i.e.*, at a fixed  $\theta$  ( $= 107.6^\circ$ ) (the open triangles), and our model calculation for various  $\phi$  and  $\theta$  (the open diamonds).

3(a). Here, the local  $z_1$  and  $z_2$  axis directions are assumed to be the same. When the orbital wavefunctions of  $\text{LaMnO}_3$  were used, it was found that the orbital rotation effect on  $S_W$  is proportional to  $\cos^2(\pi - \phi)$ . As shown in Fig. 1(c), the  $R$ -ion substitution in  $RMnO_3$  makes  $\phi$  vary from  $155.2^\circ$  to  $145.3^\circ$  [10, 20]. In Fig. 2(b), the calculated values of  $S_W$  are plotted with the open triangles. It is obvious that the variation in  $\phi$  alone cannot account for the large change in the experimental  $S_W$ .

Now, let us include the orbital mixing contribution. In a cubic  $\text{MnO}_6$  octahedron, two  $e_g$  orbitals remain doubly degenerate. Under the JT-type distortion along the  $z$ -direction, the  $e_g$  orbitals become split into two orthogonal orbitals, *i.e.*  $|3z^2 - r^2\rangle$  and  $|x^2 - y^2\rangle$ . However, a neutron scattering experiment showed that the actual occupied  $e_g$  orbital of  $RMnO_3$  should be a mixed state of these two orbitals depending on the local distortion of the  $\text{MnO}_6$  octahedron, and further that the degree of the

orbital mixing will vary depending on  $r_R$  [10]. To include the orbital mixing effects in Eq. (1), we constructed realistic Mn  $e_g$  orbitals using the orbital mixing angle  $\theta$ : the occupied orbital at site 1 and the unoccupied orbital at the neighboring site 2 are written as

$$|\psi_1^{occ}\rangle = \cos \frac{\theta}{2} |3z_1^2 - r_1^2\rangle + \sin \frac{\theta}{2} |x_1^2 - y_1^2\rangle$$

$$|\psi_2^{unocc}\rangle = -\sin \frac{\theta}{2} |3z_2^2 - r_2^2\rangle + \cos \frac{\theta}{2} |x_2^2 - y_2^2\rangle, \quad (2)$$

where the subscripts in the wavefunctions represent the different local coordinates. The unoccupied orbital, corresponding to the final state of the transition, is orthogonal to the occupied orbital at site 2. To visualize the orbital mixing effects, the occupied orbitals for three different  $\theta$  values are plotted in Fig. 3(b). [Note that the orbital configuration shown in Fig. 1(b) corresponds to  $\phi = 180^\circ$ ,  $\theta = 108^\circ$ .] From Eqs. (1) and (2), we obtained,

$$S_W \propto \left\{ \left( \sin \theta - \frac{\sqrt{3}}{2} \right) \cos(\pi - \phi) \right\}^2. \quad (3)$$

Using the reported  $(\theta, \phi)$  values from the neutron scattering experiment [10, 20], we can estimate the values of  $S_W(\theta, \phi)$  and plot them with the open diamonds in Fig. 2(b). The estimated  $S_W(\theta, \phi)$  values agree quite well with the measured  $S_W$  change, indicating the importance of the orbital mixing. The  $\theta$ - and  $\phi$ -dependence of  $S_W$  is displayed in Fig. 3(c). Note that  $\theta = 107.6^\circ$  for  $\text{LaMnO}_3$  and  $\theta = 114.3^\circ$  for  $\text{TbMnO}_3$ . Although the variation of the  $\theta$  value is about  $6.7^\circ$ , smaller than that of the  $\phi$  value (*i.e.* about  $9.9^\circ$ ), the variation of  $S_W$  due to the change in the orbital mixing is larger than that due to the  $\phi$  change. A possible reason is the strong anisotropy in the shape of the orbitals. When  $\theta = 90^\circ$ , the occupied and unoccupied orbitals given in Eq. (3) have the mean state of the two orthogonal orbitals. As  $\theta$  increases, the  $|x^2 - y^2\rangle$  orbital enhances the wavefunction overlap and the  $|3z^2 - r^2\rangle$  orbital reduces it within the  $ab$ -plane, so the mixing of those two orbitals results in the minimum around  $\theta = 120^\circ$  in Eq. (3). As shown in Fig. 3(c),  $RMnO_3$  are located near the  $(\theta, \phi)$  space where  $S_W$  will change rapidly and depend strongly on  $\theta$ . Thus, the orbital mixing becomes a crucial factor in numerous physical properties of  $RMnO_3$ , including the change in  $S_W$ .

The  $S_W$  values for various manganites are marked with the solid squares in Fig. 1(c). It is remarkable to note that the  $R$ -dependence of the  $S_W$  change is quite similar to that for  $T_N$ , *i.e.*, the  $A$ -type AFM ordering temperature. With decreasing  $R$ -ion radius ( $r_R$ ) from La to Tb,  $T_N$  systematically decreases, *i.e.* from  $\sim 140$  K for  $\text{LaMnO}_3$  to nearly zero for  $\text{TbMnO}_3$ . Similarly,  $S_W$  also becomes significantly reduced for  $\text{TbMnO}_3$  as compared with the value for  $\text{LaMnO}_3$ . These similar  $R$ -dependences of  $S_W$  and  $T_N$  are rather surprising, since

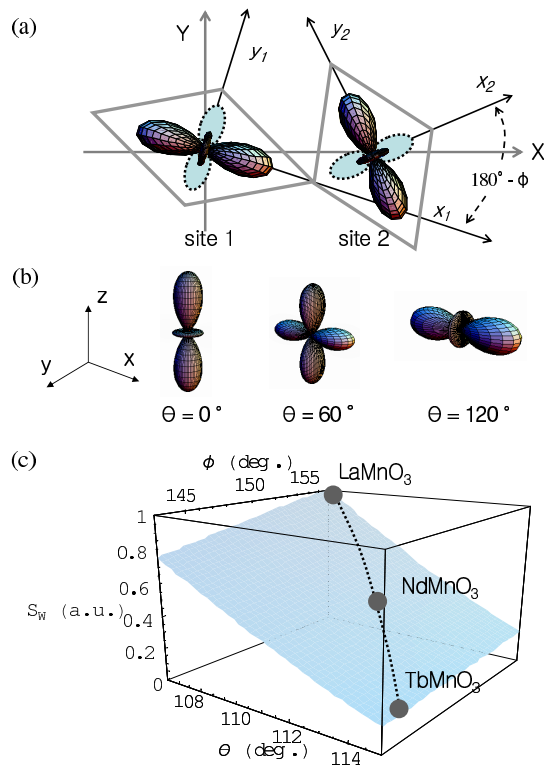


FIG. 3: (color online). The setup is schematically shown for the calculation of the orbital mixing angle ( $\theta$ ) and the Mn-O-Mn bond angle ( $\phi$ ) dependent  $S_W$ . (a) The local coordinates ( $x, y$ ) for the  $\text{MnO}_6$  octahedra and the Mn  $e_g$  orbitals (The orbital lobes drawn with the dashed lines represent the unoccupied orbitals.) (b) The occupied orbitals of selected  $\theta$  values. (c) The calculated  $S_W$  as a function of  $\theta$  and  $\phi$ .

the  $S_W$  change comes from the  $ab$ -plane response while the AFM ordering at  $T_N$  occurs along the  $c$ -axis.

One possible explanation for this intriguing phenomenon could be an occurrence of additional FM component in the inter-plane interactions due to the buckling of the  $\text{MnO}_6$  octahedra. In the undistorted case (*i.e.*,  $\phi = 180^\circ$ ), the  $A$ -type spin order should occur due to the FM  $e_g$ - $e_g$  interaction within the  $ab$ -plane and the AFM  $t_{2g}$ - $t_{2g}$  superexchange interaction along the  $c$ -axis. Here  $T_N$  is mainly determined by the latter, since it is much weaker than the  $ab$ -plane FM interaction [21]. When the buckling of the  $\text{MnO}_6$  octahedra occurs, however, the overlap of the  $e_g$ -orbitals between the Mn-planes brings out a new FM interaction along the  $c$ -axis. Although  $T_N$  of  $R\text{MnO}_3$  should be determined by the competition between the AFM and the FM interactions, the  $r_R$  dependence of  $T_N$  could be realized mostly by the latter: the AFM interaction should not be so sensitive to the structural change due to the nature of the orbitally

closed  $t_{2g}$  levels, but the FM interaction should critically depend on the buckling. Since the FM interaction does appear from the tilting of the  $\text{MnO}_6$  octahedra, it could be closely related to  $S_W$ , which will be proportional to the square of the electron hopping matrix in the  $ab$ -plane. This scenario suggests that the AFM and FM interactions will compete with each other and achieve a balance around  $\text{TbMnO}_3$ . To explain the anomalous magnetic ground states near the phase boundary, shown in Fig. 1(c), Kimura *et al.* recently used a two-dimensional anisotropic neighbor interaction model [22]. Our picture based on a new FM interaction along the  $c$ -axis might provide an alternative starting point to explain the intriguing magnetic states near the multiferroic phases.

The conventional Goodenough-Kanamori rule takes into account of the orbital overlap in terms of  $\phi$  [6, 9]. Then, the sign of the effective magnetic interactions (*i.e.* AFM and FM ground states) is expected to change near  $\phi = 135^\circ$ . In  $R\text{MnO}_3$ , the  $\text{GdFeO}_3$  type distortion can induce the competition between AFM and FM along the  $c$ -axis, so one could envisage a disappearance of AFM near  $135^\circ$ . However, as displayed in Fig. 1 (c), the  $A$ -type AFM order in the orthorhombic  $R\text{MnO}_3$  disappears at  $\phi \gtrsim 145^\circ$ . This deviation from the Goodenough-Kanamori rule should originate from the additional contribution of the orbital mixing to the orbital overlap.

In summary, we reported that the spectral weight of the 2 eV peak changes drastically with rare-earth ion size in  $R\text{MnO}_3$  ( $R=\text{La, Pr, Nd, Gd, and Tb}$ ). The spectral weight change was successfully understood in terms of the optical matrix element in which Jahn-Teller distortion and the rotation of the orbital were taken into account within the orbitally degenerate Hubbard picture. Similar behaviors between the 2 eV spectral weight and the  $A$ -type antiferromagnetic ordering temperature suggest that the superexchange interaction in  $R\text{MnO}_3$  might be tuned by the orbital degree of freedom.

We acknowledge valuable discussions with J. S. Lee, K. W. Kim, S. S. A. Seo, K. H. Ahn, P. Littlewood, and P. Horsh. This work was supported by the KOSEF CRI program and CSCMR SRC, and also supported by the Korean Ministry of Education BK21 project.

\* corresponding author: twnoh@phya.snu.ac.kr

- [1] Y. Tokura and N. Nagaosa, *Science* **288**, 462 (2000).
- [2] K. Tobe *et al.*, *Phys. Rev. B* **64**, 184421 (2001).
- [3] M. W. Kim *et al.*, *New. J. Phys.* **6**, 156 (2004).
- [4] N. N. Kovaleva *et al.*, *Phys. Rev. Lett.* **93**, 147204 (2004).
- [5] T. Inami *et al.*, *Phys. Rev. B* **67**, 045108 (2003).
- [6] J. B. Goodenough, *Phys. Rev.* **100**, 564 (1955).
- [7] T. Kimura *et al.*, *Phys. Rev. B* **68**, 060404(R) (2003).
- [8] T. Kimura *et al.*, *Nature(London)* **426**, 55 (2003).
- [9] J. Kanamori, *J. Phys. Chem. Solids* **10**, 87 (1959).
- [10] J. A. Alonso *et al.*, *Inorg. Chem.* **39**, 917 (2000).

- [11] M. W. Kim *et al.*, Phys. Rev. Lett. **89**, 016403 (2002).
- [12] J. S. Lee, M. W. Kim, and T. W. Noh, to be published.
- [13] P. Murugavel *et al.*, Appl. Phys. Lett. **82**, 1908 (2003).
- [14] The orbital ordering temperature increases as the  $R$ -ion size decreases. For more information, see Ref. [7].
- [15] J. H. Jung *et al.*, Phys. Rev. B **55**, 15489 (1997).
- [16] Its energy cost can be estimated as  $U^* - 3J_H$ , where  $U^*$  is the effective on-site Coulomb repulsion energy and  $J_H$  is the Hund's rule coupling energy. See Ref. [3, 4].
- [17] W. A. Harrison, in *Electronic structure and the properties of solids*, (W. H. Freeman and Company, San Francisco, 1980).
- [18] L. C. Lew Yan Voon and L. R. Ram-Mohan, Phys. Rev. B **47**, 15500 (1993).
- [19] P. W. Anderson, in *Magnetism I*, edited by G. T. Rado and H. Suhl (Academic Press, New York, 1963).
- [20] The values for  $\text{GdMnO}_3$  were obtained by interpolation.
- [21] K. Hirota *et al.*, J. Phys. Soc. Jpn. **65**, 3736 (1996).
- [22] This model mimics the frustration, however it does not consider the additional FM interaction along the  $c$ -axis.